COMPARISON OF HIGH-ENERGY TRAPPED PARTICLE ENVIRONMENTS AT THE EARTH AND JUPITER

Insoo Jun and Henry B. Garrett

Jet Propulsion Laboratory, California Institute of Technology

Mail Stop 122-107

4800 Oak Grove Drive, Pasadena, California 91109

Short Running Title: Radiation Environments at the Earth and Jupiter

COMPARISON OF HIGH-ENERGY TRAPPED PARTICLE ENVIRONMENTS AT THE EARTH AND JUPITER

Insoo Jun and Henry B. Garrett

ABSTRACT

The "Van Allen belts" of the trapped energetic particles in the Earth's magnetosphere were discovered by the Explorer I satellite in 1958. In addition, in 1959, it was observed that UHF radio emissions from Jupiter probably had a similar source -- the Jovian radiation belts. In this paper, the global characteristics of these two planets' trapped radiation environments and respective magnetosphere are compared and state-of-the-art models used to generate estimates of the high-energy electron (≥100 keV) and proton (≥1 MeV) populations—the dominate particles in these environments. The models used are the AP8/AE8 series for the Earth and the Divine-Garrett/GIRE model for Jupiter. To illustrate the relative magnitude of radiation effects at each planet, radiation transport calculations were performed to compute the total ionizing dose levels at geosynchronous orbit for the Earth and at Europa (Jupiter's 4th largest moon) for Jupiter. The results show that the dose-rates are ~0.1 krad(Si)/day at geosynchronous orbits and ~30 krad(Si)/day at Europa with a 2.5-mm of spherical shell aluminum shield—a factor of ~300 between the two planets.

INTRODUCTION

Radiation is ubiquitous in space. It includes low energy solar wind particles, extremely high energy galactic cosmic rays, high energy protons and heavy ions from solar energetic particle events, and charged particles trapped in planetary magnetic fields. The Sun emits an enormous amount of energy in the form of charged particles and photons associated with the 6000 ^{o}K blackbody radiation. The bulk of the flow of charged particles is in the form of the solar wind. It originates in the corona, the uppermost part of the solar atmosphere, which has a temperature of more than 10^{6} ^{o}K. Because of its high temperature, the coronal gas is ionized and forms a plasma. Typically the solar wind is supersonic and consists mainly of protons and electrons with a small percentage of He ions. The number density and velocity of the solar wind particles are typically 5-10 particles/cm^{3} and 400-500 km/s at 1 astronomical unit (AU), but can be high as ~100 particles/cm^{3} and 2500 km/s.

Cosmic rays are very high energy charged particles, originating in outer space, that travel at nearly the speed of light and strike the Earth from all directions. Most cosmic rays are the nuclei of atoms, ranging from the lightest to the heaviest elements in the periodic table. Cosmic rays also include high energy electrons, positrons, and other subatomic particles. The term "cosmic rays" usually refers to galactic cosmic rays, which originate in sources outside the solar system distributed throughout our Milky Way galaxy. About 89% of the cosmic ray nuclei are hydrogen (protons), about 10% are helium (alpha particles), and all of the rest of the elements make up the remaining 1%. The highest energy cosmic rays measured to date have had more than 10^{20} eV. Most galactic cosmic rays are probably accelerated in the blast waves of supernova remnants. This doesn't mean that the supernova explosion itself gets the particles up to these energies. The remnants of the explosions, expanding clouds of gas and magnetic field, can last

for thousands of years, and this is where cosmic rays are accelerated. Bouncing back and forth in the magnetic field of the remnant lets some of the particles randomly gain energy and become cosmic rays. Eventually they build up enough energy that the remnant can no longer contain them, and they escape into the galaxy. Surprisingly, cosmic rays have been observed at much higher energies than supernova remnants can generate–where these ultra-high-energies come from is still a big question.

Solar energetic particle events are those events when there are increased levels of protons and heavy ions produced at the sun. There are two main classes of solar energetic particle events: gradual (proton rich) and impulsive (electron-^{3}He rich). The gradual events are strongly associated with coronal mass ejections (CMEs) as they contain the same elemental abundances and ionization states as the coronal and solar wind plasma. Besides energetic ions, electrons are also observed, but the fluxes of energetic (> MeV) protons dominate. Since these proton-rich events are typically accompanied by soft X-ray emissions of relatively long duration with e-folding decay times more than tens of minutes, they are called "gradual" events. The second type of solar energetic particle event is characterized by marked enhancements of heavy ions (especially ^{3}He ions) and electrons. This type of event is typically associated with small flares or may lack a flare entirely--there is no association with CMEs. The associated flares generally have short, impulsive soft X-ray bursts, so these are also called "impulsive" events.

Finally, a magnetosphere is the region surrounding a planet within which the planet's intrinsic magnetic field controls the physical phenomena involving electrically charged particles. A radiation belt is an interior feature of a magnetosphere and comprises a population of energetic charged particles (electrons, protons, and heavy ions) durably trapped (see later) in the magnetic field of the planet. The Earth and Jupiter possess strong magnetic fields and are popular targets

for NASA missions. This paper, in particular, presents brief descriptions of the Earth's and Jupiter's magnetospheres and radiation belts. The "Van Allen belts" or trapped energetic particles in the Earth's magnetosphere were discovered by the Explorer I satellite in 1958[1]. In addition, in 1959,[2] UHF radio emissions from Jupiter were observed that probably had a similar source--the Jovian radiation belts. Here, state-of-the-art radiation belt models for each planet are used to generate estimates of the trapped particle populations. Other outer planets also possess strong, or sometimes intriguing, planetary magnetic fields and thus have their own radiation belts but are not covered in this study. The radiation transport calculations were also performed for a generic spacecraft geometry (spherical shell) using the particle spectra at geosynchronous orbit and at Europa orbit in order to illustrate the relative levels of radiation effects.

MAGNETOSPHERES

Table 1[3] lists the principle characteristics of the terrestrial and Jovian magnetospheres. As shown in this table, Jupiter is roughly 10 times the size of the Earth while its magnetic moment is 10^5 larger. As the magnetic field at the equator is proportional to the magnetic moment divided by the cube of the radial distance, the Jovian magnetic field is proportionally 100 times larger than the Earth's. An additional consideration is that the photon flux at the Earth

Table 1. The Planets' Magnetospheres

	Earth	Jupiter
Equatorial radius (km)	6.38×10^3	7.14×10^4
Magnetic moment (G-cm^3)	8.10×10^{25}	1.59×10^{30}
Rotation period (hrs)	24.0	10.0
Aphelion/perihelion (AU)	1.01/0.98	5.45/4.95

(1 AU) is ~25 times that at Jupiter (~5 AU). The differences in rotation rate is also an important factor as Jupiter spins over twice as fast as the Earth---~10 hours versus 24 hours. Given the strong magnetic field at Jupiter, this means that the cold plasma trapped in the magnetosphere is forced to co-rotate at velocities much higher than a spacecraft's orbital velocity. This is opposite to the situation at Earth where, at low altitudes, a spacecraft orbits at ~8 km/s faster than the ionospheric plasma. Co-rotation velocities can range from 30-40 km/s near Jupiter to over 100 km/s in the outer magnetospheres. In particular, at Jupiter strict co-rotation breaks down at ~200 km/s at approximately 20 Jovian radii (1 Jovian radius = 1 R_j = 71,400 km)[4]. Closely related to the co-rotation velocity is the in-situ cold plasma density variation. At the Earth, the only source is the ionosphere so that the cold plasma population falls to a few particles per cubic centimeter by 4-5 R_e. At Jupiter, the moon Io at 5.9 R_j is an additional source of cold plasma that then extends well out into the magnetosphere (~20 R_j or farther). The cold ion population at Jupiter is a key determinate of its magnetosphere. Beyond ~15 R_j this plasma resembles the Sun's solar wind as it expands outward from Jupiter dragging the magnetic field with it. Indeed, the plasma beyond ~15 R_j distorts the Jovian magnetic field so much that radiation particles cease to be trapped (see below) beyond this distance (at Earth, this break point is around 6-8 R_e). The magnetosphere of Jupiter is dominated by three factors: the magnetic field tilt (11°) relative to its spin axis, its rapid rotation, and the Jovian moon Io at 5.9 R_j. The rapid rotation of Jupiter's magnetic field forces the cold plasma to expand by centrifugal force into a giant disc. The magnetic field tilt and rotation rate cause the plasma disc to wave up and down so that at a given location plasma and radiation parameters vary radically during a 10 hour period.

RADIATION BELTS

Physics of particle trapping

To understand the trapped radiation environment at the Earth and Jupiter, one must first understand how charged particles move in their magnetic fields. This section provides a very brief overview of the fundamentals of charged particle motion so that the concepts used in modeling the radiation belts can be comprehended. To understand how charged particles become "trapped", it is necessary to review the forces that act on those particles. Except near the upper fringes of a planet's atmosphere, collisional and frictional forces on charged particles can, in general, be ignored. The two main forces (F_E and F_M) are then (units of cm-g-s, CGS, are used unless otherwise noted) the electrostatic force:

$$\overline{F}_E = q\overline{E} \tag{1}$$

and the magnetic (Lorentz) force:

$$\overline{F}_M = \frac{q}{c}\overline{V} \times \overline{B} \tag{2}$$

where q is the particle charge (including sign), c is the speed of light, $\overline{V}$ the velocity vector of the particle, $\overline{B}$ the magnetic field vector in space, and $\overline{E}$ the electric field vector in space.

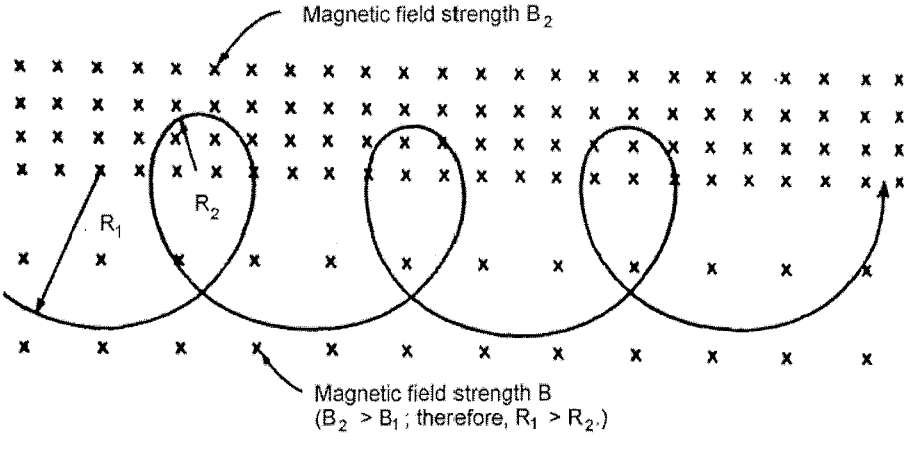

Figure 1. Motion of a charged particle (positive in this case) is illustrated in a magnetic field in the absence of an electric field.

Consider the actual motion of a particle subject to Eqs. 1 and 2. Setting the electric field to zero and using the definition of the cross product, Eq. 2 implies that the force on a charged particle is always perpendicular to both the particle's instantaneous velocity vector and the magnetic field vector. This means that a particle must, in the absence of another force and in the presence of a uniform magnetic field, move in a circle in the plane perpendicular to the magnetic field vector. It may additionally move freely (without any acceleration) along the magnetic field, mapping out a helix around its "center of motion" (Figures 1, 2, and 3). The radius R_c (called the cyclotron or gyro radius) of this circle is found by equating the centripetal force, mV^2/R, to the Lorentz force. In this expression m is the particle mass and $V_\perp$ is the component of the velocity perpendicular to B. The expression is (relativistic):

$$R_c = \frac{\gamma m_o V_\perp c}{qB} \qquad (3)$$

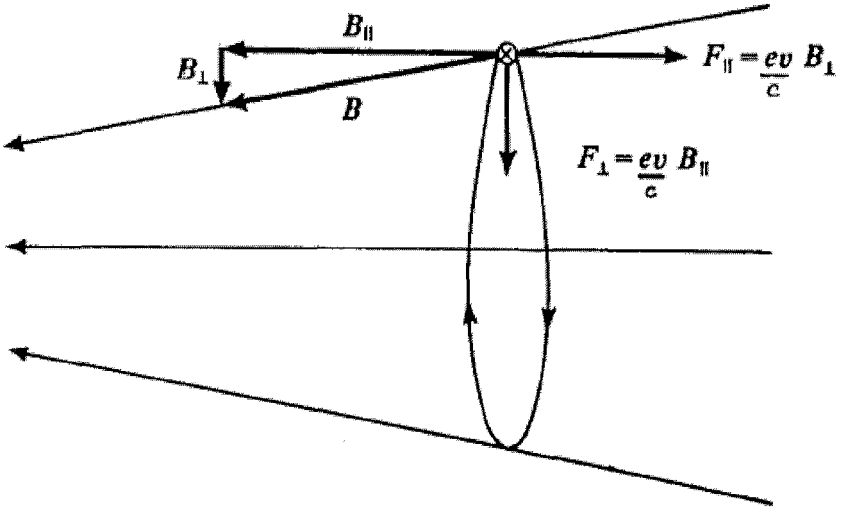

Figure 2. Motion of a charged particle is shown in a converging magnetic field in the absence of an electric field. F1 is the force along the magnetic field that results from the field convergence (or divergence) and is responsible for the mirroring effect.

The frequency with which the charged particle gyrates, the cyclotron frequency, ω_c, is given by (relativistic):

$$\omega_c = \frac{qB}{\gamma m_o c} \tag{4}$$

where ω_c is in radians per second.

According to Eq. 2, any particle motion parallel to B is unaffected by B. The particle's motion can be described in terms of a velocity parallel to the field, $V_{\|}$, or perpendicular to the field, $V_{\perp}$, and a quantity called the particle pitch angle, "α", the angle the particle motion makes relative to the B direction. It is defined as:

$$\alpha = \sin^{-1}(V_{\perp}/V) \tag{5}$$

$$\alpha = \cos^{-1}(V_{\|}/V)$$

The motion of the particle can be pictured as spiraling along the magnetic field direction, executing cyclotron motion around the field while moving along the field (Figure 3). A charged particle will deviate from these simple motions if there is an electric field or if the magnetic field has temporal changes or gradients. As an example, consider the case where the magnetic field increases with distance in a direction perpendicular to the direction of B. In this case as the particle moves from the region of low field strength to high field strength and back again, R_c decreases and increases correspondingly, and the particle traces out a cycloid configuration (Figure 1). Under the combined influence of both the Earth's electric field (this field is radially directed close to the Earth and points from dawn to dusk at greater distances) and the radial gradient of its magnetic field, charged particles will slowly trace a similar cycloid around the Earth (electrons drifting towards the east and high energy ions towards the west). Although such motion is quite complex, if the magnetic field gradient or E are sufficiently weak, the motion of

the particle can be described in terms of its cyclotron motion and a constant "drift velocity". As the particles "drift" around the Earth, bouncing back and forth on the magnetic field lines, they trace out a surface called a magnetic "L-shell" (see below for a discussion of the L value which defines the L-shell).

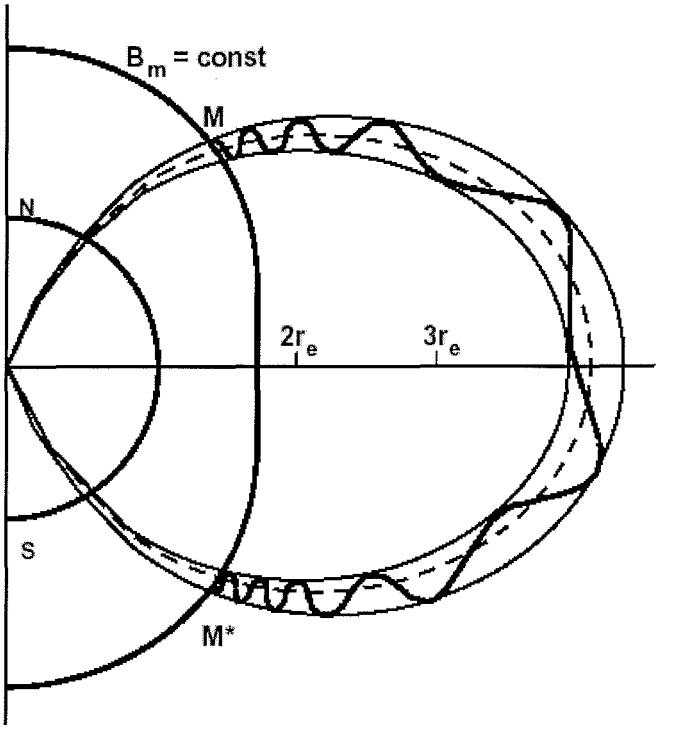

Figure 3. Motion of a charged particle in a dipole magnetic field.

The final type of motion of interest here results from gradients along the magnetic field and is responsible for the "trapping" of radiation particles in the magnetic field. If the magnetic field converges, then the particle will feel a small force along the direction of the field line. This will cause the particle to decelerate (accelerate) as it moves into the converging (diverging) region (Figure 2). Eventually (unless the particle has collisions with atmospheric particles–i.e., the mirror point is below some critical altitude which we will define by the magnetic field strength at that position, B_c), the particle will have its motion parallel to the field stopped.

However, due to the particle's circular motion (perpendicular to the field), it still experiences the decelerating force which reflects the particle back along the field line. This occurs at the "mirror" point, as determined by the strength of the magnetic field. This point is designated by "B_m" (Figure 3). B_m and B_c are critical in determining charged particle motions.

Given the preceding particle motions, it can be shown that a trapped particle's motion can be completely described to first order in terms of the magnetic field line/shell it is trapped on and where it mirrors. That is, the particle moves along a magnetic field line—the field line can be defined in terms of its "L" value. The L value is the distance, in planetary radii, where the magnetic field line crosses the magnetic equator. The magnetic field strength at which a particle mirrors, B_m, describes the pitch angle variation of the particle along the field. For slow changes in the magnetic field, the particle will stay on the same L value and mirror at the same mirror point as it slowly drifts around the Earth on a fixed L-shell. These two parameters give rise to the so-called B,L coordinate system, a common method of describing the radiation belts[5].

State-of-the-art models

There are many ways to model the radiation belts. Fortunately, the use of adiabatic invariants and the introduction of the McIlwain B-L coordinates have led to a standardized means of representing the time-averaged features of the trapped radiation environment. Although it is understood that there are many deficiencies in the models, the AE/AP series of the Earth's radiation models developed by Vette and his colleagues have been, and still are, the principal source of practical models of the Earth's trapped radiation environments. The trapped particle models in current use are the AP8[6] for protons and the AE8[7] for electrons. These models are

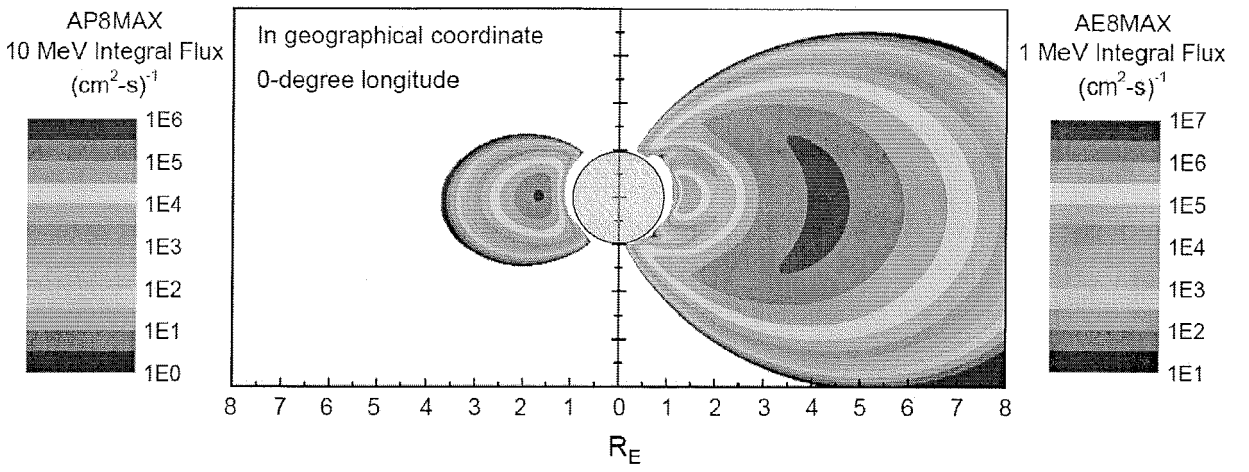

Figure 4. Contour plot showing ≥ 1MeV electron and ≥10 MeV proton integral fluxes at Earth. The coordinate system used in this plot is geographical, rather than B-L. The models used are the AP8 solar maximum model and the AE8 solar maximum model. The contour plane is for the 0-degree meridian.

empirical data sets for static conditions and provide estimates of the omni-directional fluxes of protons and electrons. The energy range of the protons included in the AP8 is 40 keV to 500 MeV. The energy range in the AE8 electron model is 40 keV to 7 MeV. The spatial range covered in the models is from low earth orbit (LEO) to somewhat beyond geo-synchronous orbit. The AP8 and AE8 models are available in two versions, one for the minimum phase of the solar cycle and one for the maximum phase. The fluxes from the models represent averages that one would expect over the solar cycle for missions of 6 months duration or longer. Other than variations in the particle fluxes due to the solar cycle phases, the models are static and do not reflect variations caused by the slowly changing geomagnetic field or due to magnetic storms and sub-storms. Uncertainty factor of $2^{(8)}$ have been defined for the AP8 and AE8. These represent the statistical uncertainty from combining data from several data sets and again do not reflect either long or short term variations in the environment. Short term variations can be

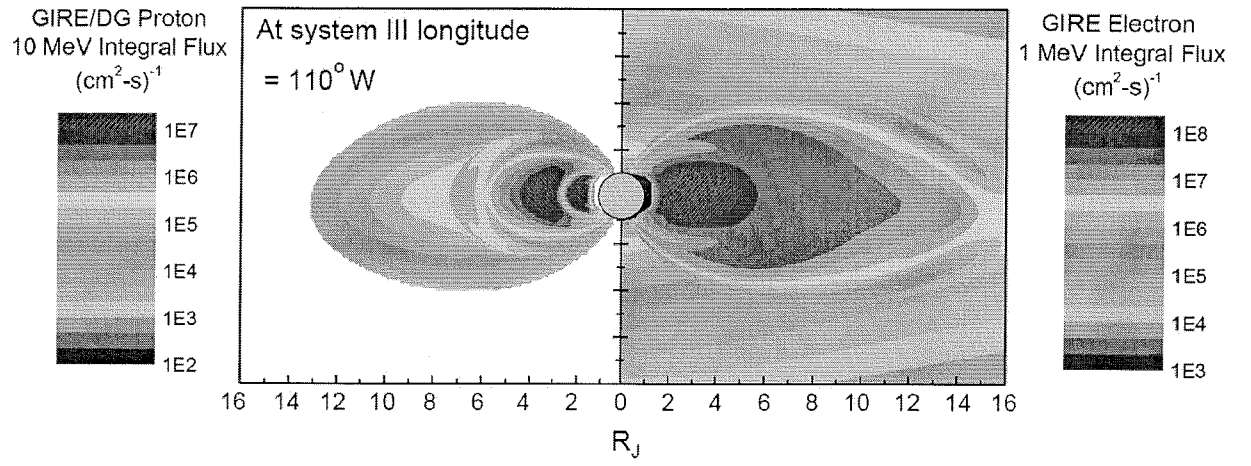

Figure 5. Contour plot showing ≥ 1MeV electron and ≥10 MeV proton integral fluxes at Jupiter. The coordinate system used in this plot is jovi-centric, rather than B-L. The models used are the AP8 solar maximum model and the AE8 solar maximum model. The contour plane is for the System III 110-degree west meridian.

orders of magnitude higher or lower from the model averages. Figure 4 for ≥ 1MeV electron and ≥10 MeV proton integral flux illustrates the basic structure of the radiation belts as predicted by the AP8 and AE8 models. The electron contours show a dual peak. Therefore, according to these models, the radiation belts are typically divided into an inner zone and an outer zone. This division also roughly corresponds, for the electrons, to an inner belt that is weakly affected by geomagnetic storms and an outer belt that is greatly affected by storms. On the other hand, the protons do not show a division into inner and outer zones.

Work on models of the energetic particle environment at Jupiter began in 1970's and was based originally on data from the Pioneer 10 and 11 spacecraft which flew by Jupiter in 1973 and 1974, respectively. The models were then refined using data returned by Voyagers I and II, both of which flew by Jupiter in 1979. For electrons and protons, this work led to the publication of the Divine-Garrett (D-G) model[4], which has been the standard Jovian radiation belt model for the

last three decades. However, the D-G model has a limitation in that the Pioneer and Voyager data on which it is based only provided quick snapshots of the Jovian magnetosphere, thus covering only a limited temporal and spatial range in the Jovian magnetosphere. Fortunately, the authors were able to use the data from the Galileo spacecraft's energetic particle detector (EPD) to refine and update the D-G electron model. Galileo provided a many-fold increase in coverage, both spatial and temporal, over the data that went into previous D-G model. The electron model developed using the Galileo EPD data is an omni-directional, equatorial model and covers the Jovian equatorial plane for the range 8 to 16 R_j. 10-minute averages of the EPD data have been used to form an extensive database of observations of the Jovian radiation belts between Jupiter orbit insertion (JOI) in 1995 and 2002. These data were then averaged to provide a differential flux spectrum at 0.174, 0.304, 0.527, 1.5, 2.0, 11.0, and 31.0 MeV in the Jovian equatorial plane as a function of radial distance. At this time, the EPD pitch angle data are still being analyzed. Pitch angle information (i.e., the particle flux relative to the magnetic field direction) is required to estimate fluxes at high latitudes. To provide this capability, the omni-directional equatorial model was merged with the D-G model pitch angle variations to provide complete latitude and L-shell coverage. This combination forms a complete model, the Galileo Interim Radiation Electron (GIRE) model[9] that can used to provide updated electron radiation environment estimates between $8 \leq L \leq 16$. The D-G model is still being used for proton environment estimates at all spatial ranges and for electron environment estimates outside the valid range of the GIRE model. Figure 5 shows a contour plot for ≥ 1 MeV electron and ≥ 10 MeV proton integral fluxes obtained using the GIRE and D-G models. As expected, the basic structure of the Jovian radiation belt is more complex than the Earth's and the flux levels are 1-2 orders of magnitude higher than those at the Earth.

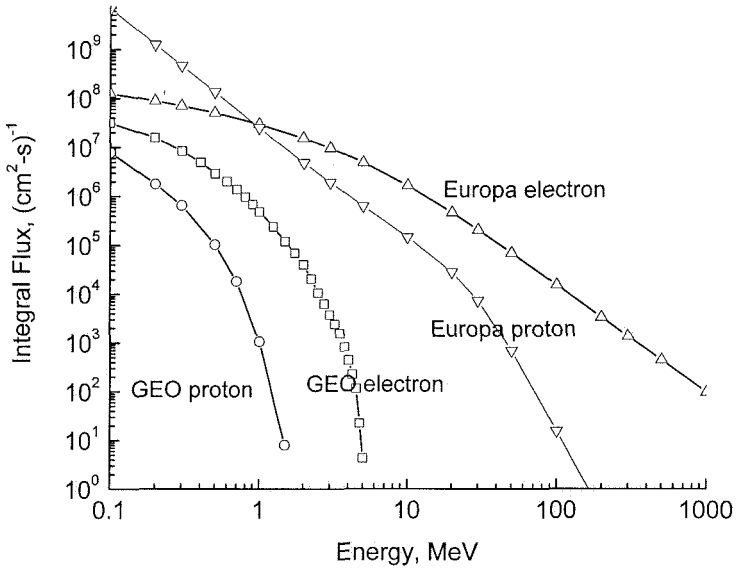

Figure 6. Trapped electron and proton spectra at geosynchronous orbit and at Europa orbit.

RADIATION TRANSPORT CALCULATIONS

The trapped electron and proton energy spectra were obtained using the radiation belt models discussed above for geosynchronous orbit (35,789 km altitude with 0° inclination) and for the Europa (9.5 Rj at Jupiter's rotational equatorial plane) orbit. The geosynchronous orbit is the orbit where most telecommunication satellites reside and Europa is one of the highest priority targets that NASA plans to send a spacecraft to in the near future. Figure 6 shows the integral spectra obtained. Again, the levels and energies of the trapped particles at Jupiter are clearly 1-2 orders of magnitude higher than the Earth's. To illustrate relative magnitude of radiation effects expected in these missions, radiation transport calculations were performed to compute the total ionizing dose for a simple, generic spacecraft geometry (aluminum spherical shell) and the results presented in "dose-depth" curves in Figure 7. Since space radiation transport calculations involve situations where radiation responses are desired for a small volume from a source

distributed over a large volume or surface, adjoint radiation transport schemes are the more efficient method. A 3-dimensional adjoint charged particle code, NOVICE([10]), was used to generate these dose-depth curves. The dose response computed is for the energy deposition in silicon, the most popular device materials used in space applications. As shown in Figure 9, the total ionizing dose levels at Europa are clearly many orders of magnitude higher than at geosynchronous orbit, especially for thick shielding (> ~0.4 cm aluminum).

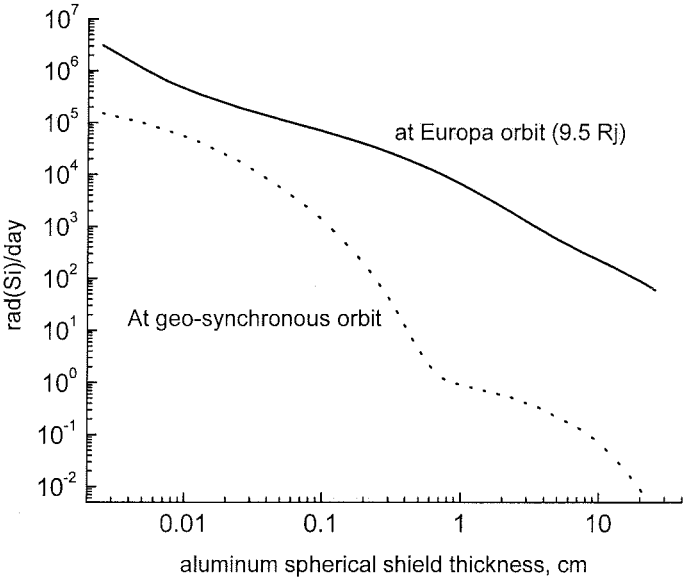

Figure 7. Total ionizing dose-depth curves corresponding to the particle spectra shown in Figure 6 as functions of aluminum spherical shell thickness.

CONCLUSION

Generic characteristics of the Earth's and Jupiter's magnetospheres were presented in this paper and the global structure of each planet's radiation belt, an interior feature of a magnetosphere, discussed in detail. State-of-the-art radiation belt models for each planet were also presented and used to generate trapped electron and proton environments. Radiation

transport calculations were performed using the trapped particle spectra for representative Earth and Jupiter orbits in order to illustrate the magnitude of radiation problems expected in missions targeting these two planets. The results showed that Jupiter's radiation environment is many orders of magnitude harsher than the Earth's in terms of the trapped particle fluxes and energy levels. The large difference in the radiation environments at these two planets implies that different techniques or design processes would be required for radiation shielding approach for missions targeting them.

ACKNOWLEDGMENT

The research described in this paper was carried out at the Jet Propulsion Laboratory, California Institute of Technology, under a contract with the National Aeronautics and Space Administration.

REFERENCES

1. Van Allen, J. A. McIlwain, C. E. and Ludwig, G. H. Journal of Geophysical Research, 64 (1959) 271.
2. F.D. Drake, H. Hvatum, Journal of Geophysical Research, 64 (1959) 329
3. Garrett, H. B. and Hoffman, A. R *Comparison of spacecraft charging environments at the Earth, Jupiter, and Saturn*, IEEE Transactions on Plasma Science, **28**(6), 2048-2057 (2000).
4. Divine, T. N. and Garrett, H. B. *Charged particle distributions in Jupiter's magnetosphere*, Journal of Geophysical Research, **88**(A9), 6889-6903 (1983).
5. McIlwain, C. E. *Coordinates for mapping the distribution of magnetically trapped particles*, Journal of Geophysical Research, **66**(11), 3681-3691 (1961).

6. Sawyer, D. M. and Vette, J. I. *AP-8 trapped proton environment for solar maximum and solar minimum*, NSSDC/WDC-A-R&S, 76-06, NASA/Goddard Space Flight Center, Greenbelt, MD (1976).
7. Vette, J. I. *The AE-8 trapped electron model environment*, NSSDC/WDC-A-R&S 91-24, NASA/Goddard Space Flight Center, Greenbelt, MD (1991).
8. Armstrong, T. E. and Colborn, B. L. *Trapped radiation model uncertainties: model – data and model – model comparisons*, NASA/CR-2000-210071, (2000).
9. Garrett, H. B. Jun, I. Ratliff, J. M. Evans, R. W. Clough, G. A. and McEntire, R. E. *Galileo Interim Radiation Electron Model*, JPL Publication 03-006 (2003).
10. Jordan, T. *NOVICE: a radiation transport/shielding code, user's guide*, Experimental and Mathematical Physics Consultants (2000).